CONF-810488--4

CONF-810488--4

DE82 013446

SIMULATED TRANSPORT OF POLYCYCLIC AROMATIC HYDROCARBONS IN ARTIFICIAL STREAMS[1]

Steven M. Bartell,[2] Peter F. Landrum,[2]
John P. Giesy,[2] and Gordon J. Leversee[2]

Abstract.--A model was constructed to predict transport of polycyclic aromatic hydrocarbons (PAH) in artificial streams. Model processes included volatilization, photolysis, sorption to sediments and particulates, and net accumulation by biota. Simulations of anthracene transport were compared to results of an experiment conducted in the streams. The model realistically predicted the concentration of dissolved anthracene through time and space. Photolytic degradation appeared to be a major pathway of anthracene flux from the streams.

DISCLAIMER

INTRODUCTION

Polycyclic aromatic hydrocarbons (PAH) are potentially hazardous by-products of the synthetic fuels industry and the generation of electricity by combustion of fossil fuels. Toxic, mutagenic (LaVoie et al. 1979), and carcinogenic (Norden et al. 1979) characteristics of PAH require estimation of human health risks posed by introduction of these chemicals into the environment.

Assessment of health risks associated with introduction of PAH into the environment depends in part upon quantification of environmental transport and subsequent dose (Crawford and Leggett 1980). Thousands of different species of PAH are chemically possible. Therefore, application of elaborate screening protocols (e.g., Duthie 1977) to identify major processes of transport, accumulation, and degradation of specific PAH is impractical for purposes of risk assessment.

This paper reports an attempt to predict the pattern of flow and accumulation of three PAH (anthracene, naphthalene, and benzo(a)pyrene) in artificial streams located on the Savannah River Plant near Aiken, South Carolina. Predictions were based upon the premise that the fundamental chemistry of individual PAH contains useful information for predictive purposes.

---

[1]Paper presented at the International Symposium on Energy and Ecological Modelling, sponsored by the International Society for Ecological Modelling (Louisville, Kentucky, April 20-23, 1981).

[2]Steven M. Bartell, Research Associate, Oak Ridge National Laboratory, Oak Ridge, Tennessee, U.S.A.; Peter F. Landrum, Research Associate, National Oceanic and Atmospheric Administration, Ann Arbor, Michigan U.S.A.; John P. Giesy, Coordinator of Aquatic Toxicology, Michigan State University, East Lansing, Michigan U.S.A.; Gordon J. Leversee, Associate Director, Savannah River Ecology Laboratory, Aiken, South Carolina U.S.A.

Predictions of transport of PAH were made for streams because energy industries that produce PAH require large volumes of water for production or cooling purposes. Thus, they are often located near streams and rivers where the probability of accidental or chronic addition of PAH to adjacent waters might be relatively high.

MODEL DESCRIPTION

Simulation of PAH transport in lotic systems requires an understanding of the basic structure and function of streams and rivers, as well as of the physical, chemical, and biological processes that determine transport of PAH compounds. Basic ecological information concerning species composition, standing crop, nutrients, and energy flow has accumulated for a variety of lotic systems (Coffman et al. 1971, Fisher and Likens 1972, McIntire and Phinney 1965, Minshall 1978, Odum 1957, Teal 1957, Tilly 1968). Yet streams and rivers have not received the attention from ecological modelers that other aquatic systems have (e.g., Patten 1968). Models of lotic systems have classically been the purview of sanitation engineers. State variables in these models included dissolved oxygen, biological oxygen demand, and total solids. Model structure represented a stream or river as a series of segments (reaches), which can be individually very different in dimensions and hydraulic characteristics, but which are assumed internally homogeneous.

Recently, some ecologists have begun to simulate energy and material flow through lotic systems, borrowing the reach-model approach (Chen and Wells 1976, Knowles and Wakeford 1978, McIntire and Colby 1978, Sandoval et al. 1976, Zalucki 1978). Our strategy was to adopt this approach.

Specific processes believed to influence PAH flux included photolytic degradation, volatilization, sorption to suspended particulates and sediments, and uptake and depuration by stream biota. These processes were incorporated into a Fates of Aromatics Model (FOAM). Figure 1 illustrates model pathways of PAH flux through a single reach.

An overall mass balance approach was taken to model the change in PAH concentration through time and space:

$$\partial P_{(t,j)} = \frac{\partial P_{(t,j)}}{\partial t} + U_{(t,j)} \frac{\partial P_{(t,j)}}{\partial j} \quad , \qquad (1)$$

where

P = PAH concentration in reach j at time t,

j = distance downstream (m), and

U = current velocity (m/t).

Equation (1) was solved by numerical approximation after conversion to difference equations (Sandoval et al. 1976). $P_{(t,j)}$ is the sum of time dependent change and advective change. Dispersion was not considered in the model. The time step (Δt) was determined by a necessary relationship between reach length and current velocity: $U \cdot \Delta t = \Delta j$ (Bella and Dobbins 1968).

Hydrological Submodel

Application of the model was constrained to conditions of constant reach geometry and constant discharge. For modeling purposes, the 91.4-m long artificial stream channel was conceptually divided into five equal reaches. Reach length was 18.28 m, width was 0.63 m, and depth was 0.20 m. The continuity equation calculated current velocity in relation to constant cross sectional area and discharge:

$$V = Q/A \quad , \qquad (2)$$

where

V = current velocity (18.28 m/h),

Q = discharge (4.53 m^3/h), and

A = reach cross sectional area (0.12 m^2).

This submodel, while simplistic, was representative of the artificial streams.

Temperature Dependent Processes

In FOAM, water temperature can influence transport of PAH through the foodweb by regulating rates of photosynthesis and respiration according to an empirically derived function (Shugart et al. 1974). Temperature gradients can be simulated using hourly input temperatures for each reach. However, for simulations reported in this study, water temperature was constant, 22°C, for all reaches.

Solar Radiation Submodel

Incident solar radiation drives photolytic degradation of PAH and photosynthesis in FOAM. A modification of Satterlund and Means' (1978) model was incorporated in FOAM to simulate daily noon light intensities used in a 12-h light:dark cycle:

$$I_t = (I_{ds} + I_s F) \cdot (1 - C) + (I_{do} + I_s)\, C e^{-d} F, \quad (3)$$

where

I_t = light intensity at reach surface (ly/h),

I_{ds} = slope dependent, direct beam radiation (ly/h),

I_s = scattered clear sky radiation (ly/h),

I_{do} = direct radiation on horizontal surface (ly/h),

C = fractional cloud cover,

F = slope correction for scattered radiation, and

d = regression parameter for seasonal cloud effects.

Light intensity at the reach surface was attenuated with water depth. Hyperbolic equations generated partial extinction coefficients for suspended particulate matter and phytoplankton.

Photolysis Submodel

Light-dependent degradation of aromatic hydrocarbons can be important in the physical-chemical transformation of PAH in aquatic systems (Southworth 1979a). Direct photochemical breakdown of dissolved PAH and degradation of photosensitized PAH sorbed to suspended particulates both occur; however, Miller and Zepp (1979) concluded that indirect photolytic degradation of sorbed PAH was minor in comparison to direct photolysis. In FOAM only direct photolysis of dissolved PAH was modeled.

In the photolysis submodel, PAH was degraded according to an equation adapted from Zepp and Cline (1977):

$$\frac{dPAH_d}{dt} = \phi \sum_{\lambda} k_{\lambda} \, PAH_d \quad , \qquad (4)$$

where

ϕ = a molar yield coefficient (unitless),

k_{λ} = light absorbed at wavelength λ, and

PAH_d = concentration of dissolved PAH (μmoles/L).

Reported yield coefficients ranged between 0.001 and 0.01 for polycyclic aromatic hydrocarbons (Zepp and Schlotzhauer 1979). A linear regression based upon data in Zepp and Schlotzhauer (1979) related molecular weight to yield coefficient:

$$\phi = 0.0235 - 8.38 \times 10^{-5} \cdot MW \quad . \qquad (5)$$

Light absorbance for specific PAH compounds was summed over 10-nm wavelength increments between 300 and 500 nm, a region of maximum absorbance for PAH. Each k_{λ} was calculated as the product of light intensity at lambda and the molar extinction coefficient for lambda, e_{λ}. Compound-specific values of e_{λ} were supplied as model input.

Light intensity, Ro, incident on each reach surface was simulated by equation (3). Light

intensity at each wavelength was attenuated as a function of depth according to a regression derived for 12 southeastern United States rivers (Zepp and Cline 1977):

$$\alpha_\lambda = 0.42e^{(-0.0044 \cdot \lambda)} \quad , \qquad (6)$$

where α_λ has units of 1/cm.

A depth-specific rate of photolysis was calculated for 1.0-cm intervals until: (1) the depth of the reach had been equaled or (2) the depth specific rate was less than 10% of the rate calculated for the 0 to 1.0 cm depth interval. Depth-specific rates were integrated over the water column and converted to units of $gPAH/m^2$. The mass of degraded PAH was added to the dissolved metabolite pool.

Modeled differences in rate of photolysis of specific PAH resulted from differences in molecular weight that translated to different molecular yield coefficients (eq. 5), and from differences in absorbance spectra.

Sorption Submodel

Karickhoff et al. (1979) modeled sorption as a first-order relationship between the concentration of dissolved PAH and an equilibrium-partition coefficient, K_p. The partition coefficient increased linearly as a function of the organic content of the sorbent material. The partition coefficient also correlated with the octanol/water partition coefficient (K_{ow}) of the PAH.

Depending upon available data, rates of sorption were calculated in one of three ways. First, if K_{ow} and the organic fraction of the sorbent were known, K_p was calculated from:

$$LOG(K_{oc}) = LOG(K_{ow}) - 0.21 \quad , \qquad (7)$$

and

$$K_p = K_{oc} \cdot oc \quad , \qquad (8)$$

where

oc = fractional organic content of the sorbent, and

K_{oc} = coefficient for partitioning into organic fraction of sorbent.

Second, if K_{ow} was not known, K_{oc} was estimated from the solubility of the particular PAH:

$$LOG(K_{oc}) = -0.54 * LOG(S) - 0.44 \quad , \qquad (9)$$

where

S = solubility of the PAH, as a mole fraction, and K_p was estimated from (8).

Third, if neither K_{ow} nor the organic fraction of the sorbent was known, a partition coefficient was estimated directly from:

$$LOG(K_p) = 4.16 - 0.51 \cdot LOG(S) \quad , \qquad (10)$$

where

S = solubility of the PAH, (ppm).

Equation (10) resulted from analysis of data in Karickhoff et al. (1979).

As a first approximation, K_p values were divided by the duration of the Karickhoff et al. (1979) experiments to convert to units of inverse time. We assumed that these values provided first estimates of a maximum rate of sorption per unit mass of sorbent, S_{max}. At each iteration of the model, specific rates of sorption were calculated for suspended particulate matter and sediments according to:

$$S = S_{max} \cdot SBATE \cdot SBENT \cdot oc/[SBATE + (SBENT \cdot oc)] \quad , \qquad (11)$$

where

S = rate of sorption (gPAH m^{-2} h^{-1}),

S_{max} = maximum sorption rate (gPAH g^{-1} h^{-1}),

SBATE = soluble PAH (g/m^2), and

SBENT = sorbent (g/m^2).

With (11), the rate of sorption was proportional to the concentration of dissolved PAH when the

concentration of the sorbent was large by comparison. Conversely, when sorbent concentration was low, sorption primarily reflected the concentration of the sorbent.

Desorption of PAH from sorbent material was not included in the sorption submodel. Net suspension of suspended particulate matter and sediments provided pathways for advective loss of sorbed PAH from each reach in the modeled stream.

Volatilization Submodel

The submodel that simulated losses of PAH from the artificial streams as a result of volatilization was taken directly from Southworth (1979b). The rate of volatilization was modeled as a function of current velocity, wind velocity, reach depth, and molecular weight of the PAH according to a hyperbolic equation involving Henry's Law:

$$K_L = H \cdot K_g \cdot K_l / [(H + K_g) \cdot K_l] , \qquad (12)$$

where

H = molar concentration of PAH in air divided by molar concentration of PAH in water,

K_g = gas phase exchange coefficient (cm/h),

K_l = liquid exchange coefficient (cm/h), and

K_L = overall transfer coefficient (cm/h).

The logarithms of H, K_g, and K_l were estimated from regressions defined in Southworth (1979b). Current velocities required by the regression equations were calculated by the hydrological submodel. Wind velocity was specified as an input parameter and was a constant 1.0 m/s in all simulations.

Biological Production Submodel

Rates of biomass change were determined by first-order, mass-balance, differential equations. The equation for producer i (phytoplankton, periphyton, macrophytes) in reach j at time t was:

$$\frac{dP_i}{dt} = (FI_i - FO_i) + P_i\,(PS_i - R_i - M_i - U_i - S_i) - G_i \quad , \tag{13}$$

where

P_i = biomass of producer i (g dry wt/m^2),

FI_i = inflow of P_i from reach j-1 (g m^{-2} h^{-1}),

FO_i = outflow of P_i to reach j+1 (g m^{-2} h^{-1}),

PS_i = rate of gross photosynthesis of P_i (g g^{-1} h^{-1}),

R_i = respiration rate (g g^{-1} h^{-1}),

M_i = non-grazing mortality rate (1/h),

U_i = secretion-excretion rate (1/h),

S_i = sinking rate (1/h), and

G_i = loss of P_i to grazing (g m^2 h^{-1}).

The mass balance equation for changes in consumer biomass (zooplankton, bacteria, benthic invertebrates, fish) was:

$$\frac{dN_i}{dt} = (FI_i - FO_i) + \sum_j C_{ij} - N_i\,(R_i + F_i + U_i + M_i) - G_i \quad , \tag{14}$$

where

N_i = biomass of consumer i in reach j at time t (g dry wt/m^2),

C_{ij} = consumption of prey j by consumer i (g m^{-2} h^{-1}),

FI_i, FO_i = same as in equation (13), but for consumer i,

R_i = respiration rate of consumer i, (g g^{-1} h^{-1}),

F_i = fraction of consumption that was egested (1/h),

U_i = excretion rate for consumer i (1/h),

M_i = non-predatory mortality rate for consumer i (1/h),

G_i = predatory losses of consumer i ($g\ m^{-2}\ h^{-1}$).

Photosynthesis.--Gross photosynthesis was modeled after Smith (1936):

$$PS_{(ijt)} = f(T) \cdot P_{max} \cdot I \cdot (I_k^2 + I^2)^{1/2} \quad , \quad (15)$$

where

PS_{ijt} = grams photosynthesized per gram producer at time t in reach j by producer i,

P_{max} = light saturated photosynthetic rate for i ($g\ ly^{-1}\ h^{-1}$),

I = light intensity from solar submodel (ly/h),

I_k = light saturation constant for producer i (ly/h), and

$f(T)$ = temperature dependence of photosynthesis.

Respiration.--For producers, a fraction of gross photosynthesis, or for consumers, a fraction of consumption, was lost through respiration.

Consumption.--PAH moved through the foodweb by the feeding activities of the consumer components. Consumption was modeled as a function of predator and prey biomass (DeAngelis et al. 1975):

$$C_{i,j} = f(T) \cdot \frac{C_{max\ i} \cdot N_i \cdot w_{ij} \cdot N_j \cdot \rho_j}{N_i + \sum_j (w_{ij} \cdot N_j \cdot \rho_j)} \quad , \quad (16)$$

where

$C_{i,j}$ = biomass of prey j consumed by consumer i ($g\ m^2\ h^{-1}$),

$C_{max\ i}$ = maximum feeding rate of consumer i, ($g\ g^{-1}\ h^{-1}$),

N_i = biomass of consumer i (g/m^2),

N_j = biomass of prey j (g/m^2),

w_{ij} = Bayesian preference of consumer i for prey j (unitless),

$f(T)$ = temperature dependence of predation (eq. 4), and

ρ_j = PAH concentration of prey j (gPAH/g dry wt).

This equation has been usefully applied to models of feeding of zooplankton, benthic invertebrates and fish (Kitchell et al. 1974, O'Neill 1976, and Smith et al. 1975).

Excretion.--At each iteration a fraction of biomass and its PAH content were excreted from each primary producer and consumer component. It was assumed that 25% of the excretory products was a metabolic product that was shunted to the metabolite pool. The remainder was excreted into the dissolved PAH pool.

Mortality.--Nonpredatory mortality was modeled in a linear, donor-dependent manner. Biomass of dead planktonic components was added to the suspended detritus pool. Nonplanktonic mortality was added to the sediments. Loss of PAH from biota was the product of biomass lost to mortality and the PAH concentration of the biomass.

Sinking Losses.--Losses of PAH from the water column due to sinking phytoplankton were modeled in a linear fashion. In FOAM the sinking rate was not coupled to the current velocity.

Egestion Losses.--A fraction of ingested food was egested by the consumer components of the model. Losses due to egestion were added to the suspended particulate pool. Egested PAH was simulated as the product of egestion rate and the PAH concentration of the food item egested.

Direct PAH Uptake.--Uptake of dissolved PAH by the primary producers in FOAM was modeled as a second-order process:

$$PU_i = P_i \cdot UP_i \cdot PAH_d/(KP_i + PAH_d) \quad , \qquad (17)$$

where

PU_i = uptake by producer i ($gPAH\ m^{-2}\ h^{-1}$),

P_i = biomass of producer i ($g\ dry\ wt/m^2$),

UP_i = maximum uptake rate ($gPAH\ g\ dry\ wt^{-1}\ h^{-1}$),

PAH_d = dissolved PAH concentrations ($gPAH/m^2$), and

KP_i is analagous to half the saturation constant ($gPAH/m^2$).

Direct uptake was assumed independent of rates of photosynthesis or respiration.

Direct uptake of PAH by consumers was coupled to the rate of respiration, assuming that uptake occurred across respiratory membranes and was an active process:

$$CU_j = N_j \cdot UC_j \cdot R_j \cdot PAH_d/(KC_j + PAH_d) \quad , \qquad (18)$$

where

CU_j = uptake of dissolved PAH ($gPAH\ m^{-2}\ h^{-1}$),

NC_j = biomass of consumer j ($g\ dry\ wt/m^2$),

UC_j = maximum uptake per unit respiration,

R_j = g dry wt respired per g dry wt,

PAH_d = dissolved PAH (gPAH m^2), and

KC_j is analagous to half saturation constant (gPAH m^2).

As an initial assumption, values of KP_i and KC_j were all defined as half of the maximum solubility of the particular PAH.

Degradation of PAH.--Metabolic degradation of assimilated PAH was modeled as a function of respiration rate and was therefore indirectly affected by water temperature.

$$D_i = R_i \cdot P_i \cdot h_i \cdot D_{max\ i} \quad , \qquad (19)$$

where

$D_{max\ i}$ = gPAH degraded h^{-1} g dry wt^{-1} respired by component i

P_i = g dry wt/m^2 of component i, and

h_i = fractional PAH content of P_i.

Metabolically degraded PAH was added to the metabolite pool.

External Loading of PAH and Solubility

Polycyclic aromatic hydrocarbons were added to the headwaters of the artificial streams. FOAM structure reflects this practice; dissolved PAH entered the first reach in the modeled stream as the product of a predefined discharge regime (m^3/h) and the PAH concentration of the influent (gPAH/m^3).

A relationship between PAH molecular weight and solubility of specific compounds was derived from data in Braunstein et al. (1977):

$$LOG(PAH_d) = 6.50 - 0.04 \cdot MW \quad , \qquad (20)$$

where

PAH_d = dissolved PAH (mg/ml), and

MW = molecular weight.

This regression was used to estimate solubility for individual PAH compounds and to ensure that solubility was not exceeded during the course of a simulation. PAH in excess of solubility was added to the sediments.

Model Parameters

Parameters for physical/chemical processes of PAH flux were estimated from data presented in papers referenced in sections that describe physical/chemical submodels.

Parameters for biological pathways of uptake and depuration result from experiments in laboratory microcosms with ^{14}C-PAH tracers and various components of the stream biota (Leversee et al. 1981).

Initial Conditions

Initial biomass conditions for the simulations were estimated from samples collected from the artificial stream or measured directly before organisms were added to the stream. Periphyton biomass was estimated as 0.18 g dry wt/m^2 in all reaches. Biomass of papershell clams (Anodonta imbecilis) was 9.31 g dry wt/m^2 in reach 1 and 8.80 in reach 5. Clams were added only to reaches 1 and 5. Bluegill sunfish were constrained by cages to reaches 1 and 5; biomass was 0.64 and 0.66 g dry wt/m^2. Bacteria biomass was estimated as 0.1 g dry wt/m^2 for all reaches. Biomass of settled detritus was arbitrarily defined as 0.5 g dry wt/m^2. The mass of active sediments was estimated as 1.0 g dry wt/m^2.

RESULTS

Simulated and Observed Transport of Anthracene

During simulated daylight hours of the 12L:12D cycle, the model predicted a downstream gradient of dissolved anthracene. Between reaches 1 and 5, a distance of 81 m, the modeled anthracene concentration decreased from 0.056 to 0.036 µmoles/liter. In the simulation, this

gradient was absent at night. FOAM predictions agreed with measured concentrations in water samples collected at midday and at dawn from the artificial streams (table 1). After termination of the addition of anthracene, predicted concentrations of dissolved anthracene decreased to zero within eight hours. Measured concentrations of anthracene decreased to below detection limits (250 nmol/L) in the channel within 24 h.

Predicted uptake of anthracene by periphyton approached a steady-state concentration of approximately 0.17 µmol/g dry weight by day 3 of the simulation (figure 2). Concentration of anthracene in periphyton exhibited a downstream gradient in the simulation. Simulated concentrations were consistently higher at night. The predicted concentrations were nearly four times higher than concentrations (0.04 µmol/g dry weight) measured in periphyton samples collected from the stream. Half-life of anthracene calculated from the simulation after the end of the infusion period was approximately 17 h, which was within 2 to 3 hours of the value calculated from measurements made on periphyton in the stream.

Figure 3 illustrates comparison of predicted and measured concentration of anthracene in the papershell clam (A. imbecilis). FOAM predicted the general pattern of the time-dependent uptake and depuration of anthracene. However, the model underestimated the actual rates of uptake and depuration by a factor of approximately 1.5. The downstream gradient predicted by the model was not supported by the data.

The model predicted a linear rate of increase in anthracene concentration in stream sediments during the course of the simulation. Estimated steady-state values approximated 0.090, 0.004, and 0.003 µmol/g dry weight in reaches 1, 3, and 5, respectively (table 2). FOAM failed to predict the pattern of uptake and release of anthracene from the sediments as measured concentrations decreased after termination of the anthracene infusion to the stream. FOAM also underestimated the rate of uptake. The model did, however, predict a downstream gradient in sedimented anthracene similar to the measured gradient.

Figure 4a illustrates the relative importance of non-advective physical/chemical processes versus biological processes in determining the flux of anthracene through the simulated lotic system. The periodic behavior in figure 4a corresponded to the light:dark cycle and emphasizes the importance of photolyic degradation of anthracene in overall transport. As more anthracene entered the food web during the simulation, the biological processes became increasingly important. Of the modeled processes, egestion and defecation of anthracene by consumers dominated the biological flux of compound in the stream. After the end of the infusion period, anthracene flux was completely dominated by biological processes.

Naphthalene and Benzo(a)pyrene Simulations

The initial premise stated that the transport and fate of specific PAH compounds could be predicted from basic chemistry of the compounds. Given some agreement between simulated and measured fate of anthracene in the artificial stream channel, the experiment was simulated again, this time with equal infusion rates for naphthalene and benzo(a)pyrene. Initial conditions and parameter estimates were identical to those for the anthracene simulation. Only values of molecular weight and absorbance spectra were changed to correspond to either naphthalene or benzo(a)pyrene.

Without data for comparison with FOAM simulations, discussion of the dynamics of individual state variables becomes rather meaningless. However, it is reasonable to examine the relative importance of various pathways of simulated flux in light of available information concerning observed behavior of these compounds in natural or experimental systems. The simulated fate of naphthalene was similar to that of anthracene with respect to the relative importance of physical/chemical versus biological processes. Figure 4b shows that physical/chemical processes accounted for more than 90% of naphthalene flux through the model system. However, the absence of periodic behavior corresponding to the light-dark cycle indicated that, unlike anthracene, photolysis was

not the dominant process. Closer inspection of the data summarized by figure 4b revealed that volatilization was the major physical/chemical pathway of naphthalene loss from the simulated stream. Lee et al. (1978) concluded that evaporation was an important process in the overall loss of naphthalene from large pelagic enclosures. Similar to the anthracene simulation, the processes of consumer egestion and defecation assumed importance in the overall flux of naphthalene following the termination of naphthalene infusion to the simulated stream.

The transport of benzo(a)pyrene (BaP) was dominated by biological processes, in contrast to the lighter weight anthracene and naphthalene (figure 4c). Following an initial 8-h period of infusion where photolytic degradation was important, uptake by primary producers, movement through the foodweb, and consumer processes of egestion and defecation played the determining role in the non-advective transport and fate of BaP in the modeled stream. Lu et al. (1977) observed biomagnification of BaP by biota in a simple aquatic microcosm that contained algae, mosquito larvae, Daphnia, snails, and fish. Lee et al. (1978) found 40% of BaP added to marine pelagic enclosures in samples of sediments. Of the physical/chemical processes simulated, sorption to suspended particulates and settled sediments was the most important vector simulated for BaP by FOAM.

DISCUSSION

The modeling effort attempted to evaluate the usefulness of molecular weight for predicting transport of individual PAH compounds. Molecular weight was correlated with water solubility, eq. (20), photolytic molar yield coefficient, eq. (5), rate of sorption (indirectly), eq. (10), and gas-phase exchange coefficient in volatilization, eq. (12) (Southworth 1979b).

The absence of rate coefficients for biological transport processes in relation to molecular weight or other fundamental chemical properties of PAH reflected the limited amount of data available for estimation of such correlations. Therefore, the model depended on

extrapolation of rate constants measured in the laboratory or published in the literature. As the number of necessary rate parameters that must be directly measured in the system of interest increases, specific application of transport models becomes more difficult (e.g., Baughman and Lassiter 1978).

Results of initial simulations indicated that FOAM predicted the observed spatial-temporal dynamics of dissolved anthracene with reasonable accuracy (table 1). This agreement might simply reflect the comparative sophistication of the photolytic submodel and the susceptibility of anthracene to photolytic degradation (Zepp and Schlotzhauer 1979, Southworth 1979a).

Lack of close agreement between simulated and measured concentrations of anthracene in periphyton, clams, and sediments indicates the difficulties in extrapolating laboratory determined rate constants to the streams. For example, rate of uptake by periphyton was overestimated. The cultures of algae used in the laboratory experiments to determine uptake did not resemble the species composition of the flora that was growing in the experimental stream.

While data from the stream were not available for comparison, simulations of naphthalene and BaP transport demonstrated that the model was sensitive to changes in parameters that determined PAH transport in relation to molecular weight and light absorbance. Furthermore, the general patterns of flux predicted by the model for these two compounds agreed qualitatively with observations made on other aquatic systems (Lee et al. 1978, Lu et al. 1977).

Results of this initial modeling effort suggest that:

(1) rate of physical/chemical processes of PAH transport in lotic systems can be predicted from molecular weight of individual compounds,

(2) light absorbance spectra between 300 and 500 nm contain information for predicting rates of photolytic degradation of PAH and

(3) parameters for biological transport and accumulation of PAH can be extrapolated to artificial streams with limited success.

The modeling effort suggested that future work is required in the following areas:

(1) collection of data to examine possible relationships between PAH compound structure and rates of biological uptake, degradation, and depuration, and

(2) collection of data in additional monitoring experiments for comparison with model predictions.

Results of this suggested research will increase our ability to predict exposure and dose in an overall assessment of risk associated with introduction of PAH into aquatic systems.

ACKNOWLEDGEMENTS

This work continues under Interagency Agreement EPA-79-d-X0290-1 with the Environmental Protection Agency and the Department of Energy, under contract EY-A-09-0943 between the University of Georgia and the Department of Energy, and by Oak Ridge National Laboratory operated by Union Carbide Corporation under contract W-7405-eng-26 with the Department of Energy. Publication No. ____, Environmental Sciences Division. Without the help of T. Fannin, S. Gerould, J. Haddock, M. Bruno, J. Bowling, J. Cheetam, S. Giddings, and R. Schloesser in the experimental phase of this project, the modeling effort would have been impossible. Comments made by G. R. Southworth, J. M. Giddings, and W. Van Winkle on earlier drafts were greatly appreciated.

LITERATURE CITED

Baughman, G. L., and R. R. Lassiter. 1978. Prediction of environmental pollution concentration p. 35-54. In Cairns, J., K. L. Dickson, and A. W. Maki, (eds.), Estimating the hazard of chemical substances to aquatic life. ASTM STP, American Society for Testing and Materials. 657 p.

Bella, D. A., and W. E. Dobbins. 1968. Difference modeling of stream pollution. J. Sanitary Engineering ASCE 94:995-1016.

Braunstein, H. M., E. D. Copenhaver, and H. A. Pfuderer, editors. 1977. Environmental, health, and control aspects of coal conversion: an information overview. ORNL/EIS-94, Oak Ridge National Laboratory, Oak Ridge, Tennessee.

Chen, C. W., and J. T. Wells, Jr. 1976. Boise River ecological modeling. p. 171-203. In R. P. Canale (ed.), Modeling biochemical processes in aquatic ecosystems. 389 p. Ann Arbor Science Inc., Ann Arbor, Michigan..

Coffman, W. P., K. W. Cummings, and J. C. Wuycheck. 1971. Energy flow in a woodland stream ecosystem: tissue support structure of the autumnal community. Arch. Hydrobiol. 68:232-276.

Crawford, D. J., and R. W. Leggett. 1980. Assessing the risk of exposure to radioactivity. Amer. Sci. 68:524-536.

DeAngelis, D. L., R. A. Goldstein, and R. V. O'Neill. 1975. A model for trophic interaction. Ecology 56:881-892.

Duthie, J. R. 1977. The importance of sequential assessment in test programs for estimating hazard to aquatic life. pp. 17-35. In Mayer, F. L. and J. L. Hamelink (eds.), Aquatic toxicology and hazard evaluation. 307 p. ASTM STP 634, American Society for Testing and Materials.

Fisher, S. G., and G. E. Likens. 1972. Stream ecosystem: organic energy budget. BioScience 22:33-35.

Karickhoff, S. W., D. S. Brown, and T. A. Scott. 1979. Sorption of hydrophobic pollutants to natural sediments. Wat. Res. 13:241-248.

Kitchell, J. F., J. F. Koonce, R. V. O'Neill, H. H. Shugart, Jr., J. J. Magnuson, and R. S. Booth. 1974. Model of fish biomass dynamics. Trans. Amer. Fish. Soc. 103:786-798.

Knowles, G., and A. C. Wakeford. 1978. A mathematical deterministic river-quality model. Part I: Formulation and description. Wat. Res. 12:1149-1153.

LaVoie, E., L. Tulley, V. Bedenko, and D. Hofman. 1979. Mutagenicity, tumor initiating activity and metabolism of tricyclic polynuclear aromatic hydrocarbons (abstract). In Jones, P. W. and P. Leber (eds.), Polynuclear Aromatic Hydrocarbons. 892 p. Ann Arbor Sciences, Ann Arbor, Michigan.

Lee, R. F., W. S. Gardner, J. W. Anderson, J. W. Blaylock, and J. Barxwell-Clarke. 1978. Fate of polycyclic aromatic hydrocarbons in controlled ecosystem enclosures. Environ. Sci. Technol. 12:832-838.

Leversee, G. J., J. P. Giesy, P. F. Landrum, S. Bartell, S. Gerould, M. Bruno, A. Spacie, J. Bowling, J. Haddock, and T. Fannin. 1981. Disposition of benzo(a)pyrene in aquatic systems components: periphyton, Chironomids, Daphnia, fish. In Cooke, M. and A. J. Dennis (eds.), Chemical analysis and biological fate: polynuclear aromatic hydrocarbons. Proceedings of symposium, Battelle Laboratories, Columbus, Ohio, October 19-22, 1980.

Lu, P., R. L. Metcalf, N. Plummer, and D. Mandel. 1977. The environmental fate of three carcinogens: benzo(a)pyrene, benzidine, and vinyl chloride evaluated in laboratory model ecosystems. Arch. Environ. Contam. Toxicol. 6:129-142.

McIntire, C. W., and J. A. Colby. 1978. A hierarchical model of lotic ecosystems. Ecol. Monogr. 48:167-190.

McIntire, C. D., and H. K. Phinney. 1965. Laboratory studies of periphyton production and community metabolism in lotic environments. Ecol. Monogr. 35:237-258.

Miller, G. C., and R. G. Zepp. 1979. Effects of suspended sediments on photolysis rates of dissolved pollutants. Wat. Res. 13:453-459.

Minshall, G. W. 1978. Autotrophy in stream ecosystems. BioScience 28:767-771.

Norden, B., U. Edlund, and S. Wold. 1979. Carcinogenicity of polycyclic aromatic hydrocarbons studied by SIMCA pattern recognition (abstract). In Jones, P. W. and P. Leber, (eds.), Polynuclear Aromatic Hydrocarbons. 892 p. Ann Arbor Sciences, Ann Arbor, Michigan.

Odum, H. T. 1957. Trophic structure and productivity of silver springs. Ecol. Monogr. 27:55-112.

O'Neill, R. V. 1976. Ecosystem persistence and heterotrophic regulation. Ecology 57:1244-1253.

Patten, B. C. 1968. Mathematical models of plankton production. Int. Rev. Ges. Hydrobiol. 53:357-408.

Sandoval, M., F. H. Verhoff, and T. H. Cahill. 1976. Mathematical modeling of nutrient cycling in rivers, p. 25-232. In Canale, R. P. (ed.), Modeling biochemical processes in aquatic ecosystems. 389 p. Ann Arbor Science, Inc., Ann Arbor, Michigan. p. 389.

Satterlund, D. R., and J. E. Means. 1978. Estimating solar radiation under variable cloud conditions. For. Sci. 24:363-373.

Shugart, H. H., R. A. Goldstein, and R. V. O'Neill. 1974. TEEM: A terrestrial ecosystem energy model for forests. Oecol. Plant. 25:251-284.

Smith, E. L. 1936. Photosynthesis in relation to light and carbon dioxide. Proc. Nat. Acad. Sci. 22:504-511.

Smith, O. L., H. H. Shugart, R. V. O'Neill, R. S. Booth, and D. C. McNaught. 1975. Resource competition and an analytical model of zooplankton feeding on phytoplankton. Nat. 109:571-591.

Southworth, G. R. 1979a. Transport and transformations of anthracene in natural waters. p. 359-380. In L. L. Marking and R. A. Kimerle (eds.), Aquatic Toxicology. 480 p. ASTM STP 667, American Society for Testing and Materials.

Southworth, G. R. 1979b. The role of volatilization in removing polycyclic aromatic hydrocarbons from aquatic environments. Bull. Environ. Contam. Toxicol. 21:507-514.

Teal, J. M. 1957. Community metabolism in a temperate cold spring. Ecol. Monogr. 27:283-302.

Tilly, L. J. 1968. The structure and dynamics of Cone Spring. Ecol. Monogr. 38:169-197.

Zalucki, M. P. 1978. Modeling and simulation of the energy-flow through Root Spring, Massachusetts. Ecology 59:654-659.

Zepp, R. G., and D. M. Cline. 1977. Rates of direct photolysis in aquatic environments. Environ. Sci. Technol. 11:359-366.

Zepp, R. G., and P. F. Schlotzhauer. 1979. Photoreactivity of selected aromatic hydrocarbons in water p. 141-148. In Jones, P. W. and P. Leber (eds.), Polynuclear Aromatic Hyudrocarbons, 892 p. Ann Arbor Sciences, Ann Arbor, Michigan.

LIST OF TABLES

Table 1. Predicted and observed concentrations of dissolved anthracene in artificial stream channels.

Table 2. Comparison of predicted and observed concentrations of anthracene in stream sediments.

Table 1.--Observed and predicted concentrations (μmol/L) of dissolved anthracene in artificial stream channels.

Time		Stream reach 1	3	5
Dawn				
	Observed	0.066	0.065	0.063
	Predicted	0.056	0.056	0.055
Midday				
	Observed	0.067	0.045	0.028
	Predicted	0.056	0.045	0.036

Table 2.--Comparison of observed and predicted concentrations (µmol/g dry weight) of anthracene in stream sediments.

Time (h)	Stream reach					
	1		3		5	
	Obs	Pre	Obs	Pre	Obs	Pre
24	0.0024	0.00026	0.0023	0.00020	0.0021	0.00017
48	0.0044	0.00059	0.0040	0.00045	0.0034	0.00037
96	0.0070	0.0014	0.0060	0.00096	0.0053	0.00080
168	0.0096	0.0027	0.0086	0.0018	0.0073	0.0015
336	0.0149	0.0073	0.0134	0.0040	0.0123	0.0033
360	0.0137	0.0079	0.0118	0.0041	0.0106	0.0034
384	0.0108	0.0084	0.0104	0.0043	0.0104	0.0035
432	0.0113	0.0092	0.0116	0.0044	0.0107	0.0035
528	0.0092	0.0096	0.0076	0.0044	0.0065	0.0035
672	0.0072	0.0092	0.0065	0.0042	0.0053	0.0034

LIST OF FIGURES

Figure 1. Flow chart indicating components, pathways, and processes for PAH transport within a stream segment.

Figure 2. Simulated concentration of anthracene in periphyton through time in reaches 1 and 5. Stippled area contains transient concentrations for reaches 2 to 4.

Figure 3. Simulated concentration of anthracene in the papershell clam (Anodonta imbecilis) in reaches 1 (solid line) and 5 (dashed line). Solid dots are measured concentrations for clams collected from reach 1. Open circles are measured concentrations for clams collected from reach 5.

Figure 4. Relative importance of non-advective physical/chemical processes (solid dots, dashed line) and biological processes (open circles, solid line) in total transport of (a) anthracene, (b) naphthalene, and (c) benzo(a)pyrene through artificial streams.

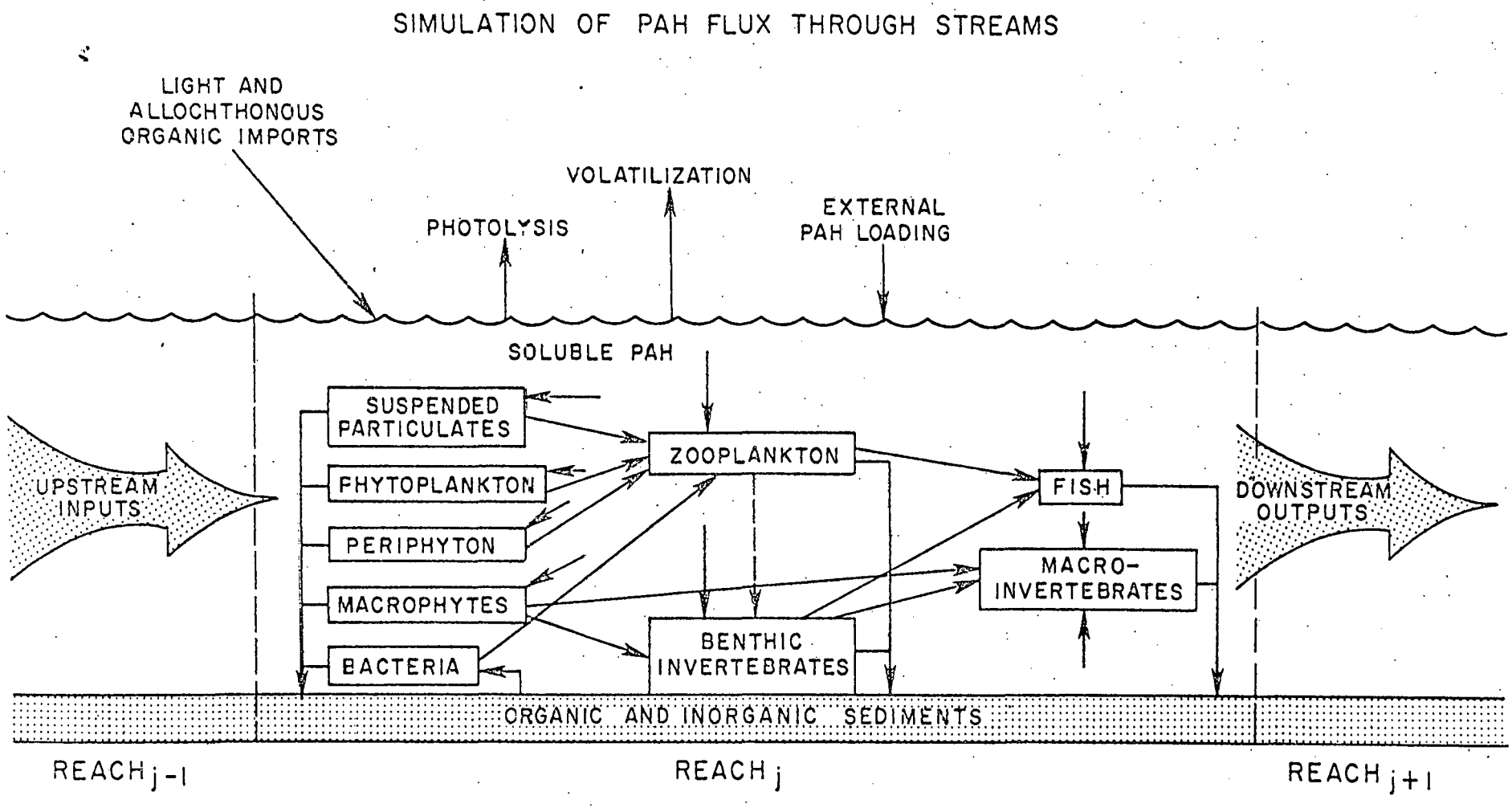
SIMULATION OF PAH FLUX THROUGH STREAMS
LIGHT AND ALLOCHTHONOUS ORGANIC IMPORTS
VOLATILIZATION
PHOTOLYSIS
EXTERNAL PAH LOADING
SOLUBLE PAH
SUSPENDED PARTICULATES
PHYTOPLANKTON
PERIPHYTON
MACROPHYTES
BACTERIA
ZOOPLANKTON
BENTHIC INVERTEBRATES
FISH
MACRO-INVERTEBRATES
UPSTREAM INPUTS
DOWNSTREAM OUTPUTS
ORGANIC AND INORGANIC SEDIMENTS
REACH j-1
REACH j
REACH j+1

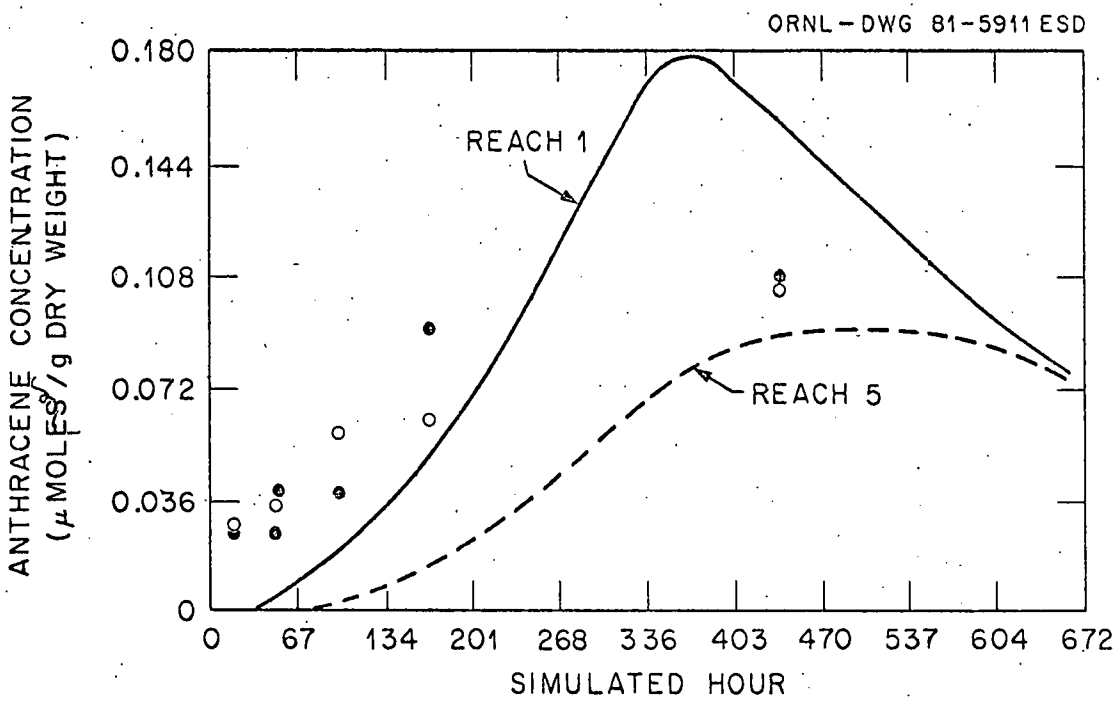
ORNL-DWG 81-5911 ESD
ANTHRACENE CONCENTRATION
(μMOLES/g DRY WEIGHT)
0.180
0.144
0.108
0.072
0.036
0
REACH 1
REACH 5
0
67
134
201
268
336
403
470
537
604
672
SIMULATED HOUR

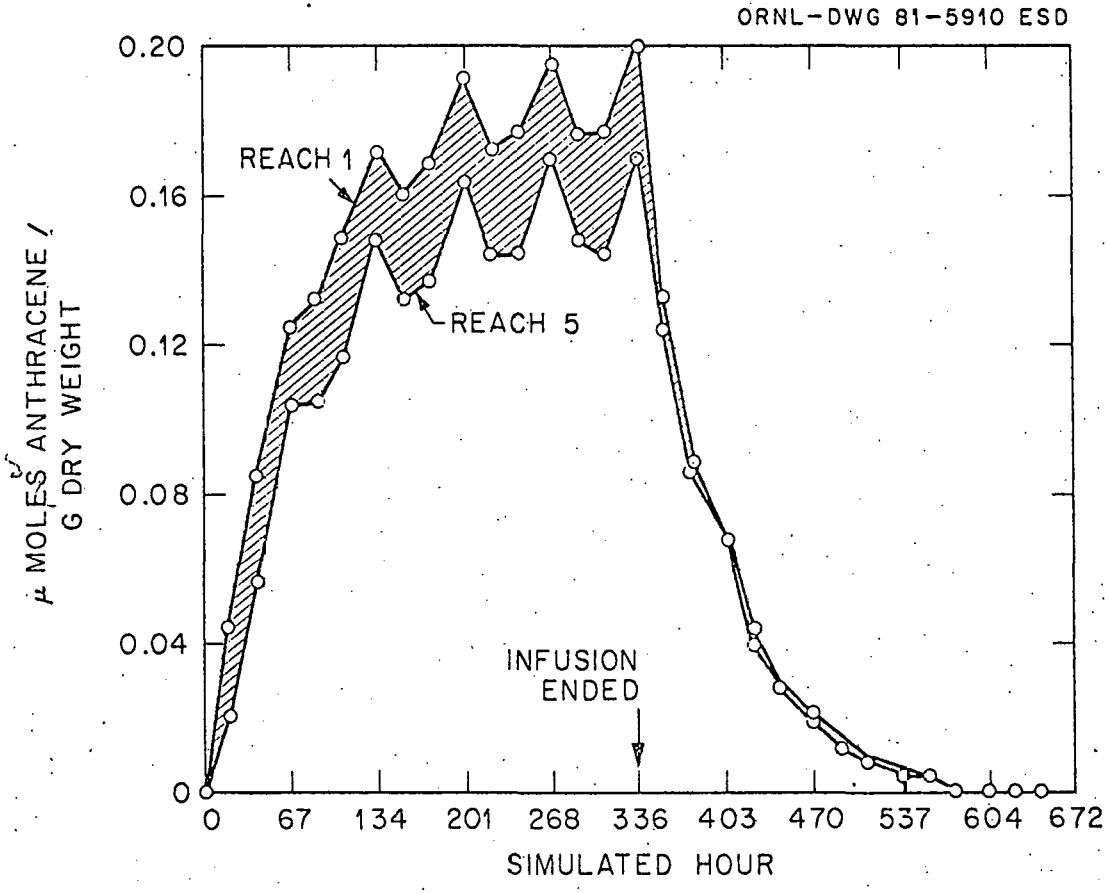
ORNL-DWG 81-5910 ESD
0.20
0.16
0.12
0.08
0.04
0
REACH 1
REACH 5
INFUSION ENDED
0
67
134
201
268
336
403
470
537
604
672
SIMULATED HOUR
μ MOLES ANTHRACENE / G DRY WEIGHT

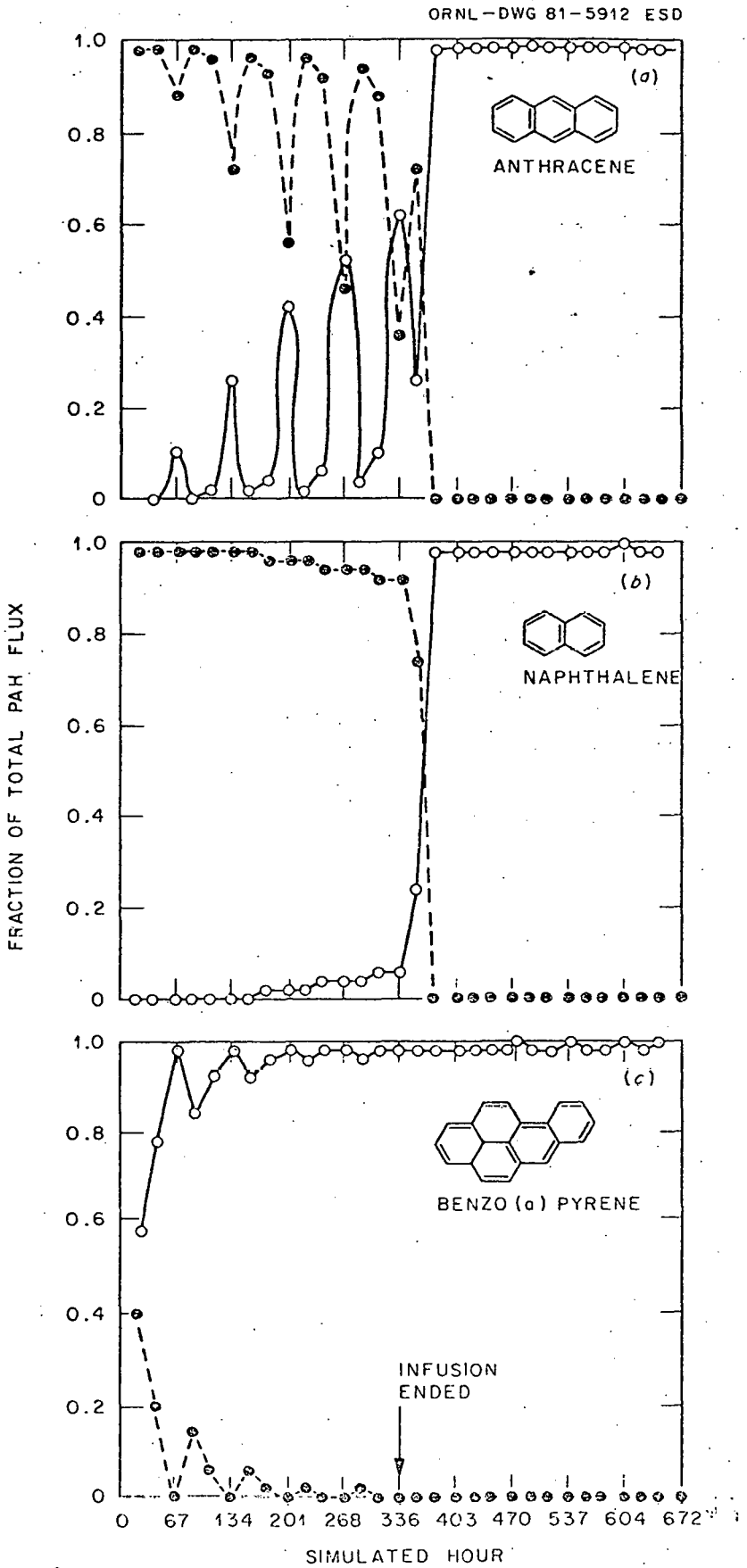
ORNL-DWG 81-5912 ESD
(a)
ANTHRACENE
(b)
NAPHTHALENE
(c)
BENZO (a) PYRENE
INFUSION ENDED
FRACTION OF TOTAL PAH FLUX
SIMULATED HOUR
0
0.2
0.4
0.6
0.8
1.0
0
67
134
201
268
336
403
470
537
604
672